Defective phagosome motility and degradation in cell nonautonomous RPE pathogenesis of a dominant macular degeneration

Julian Esteve-Rudd[a,1], Roni A. Hazim[a,1], Tanja Diemer[a], Antonio E. Paniagua[a], Stefanie Volland[a], Ankita Umapathy[a], and David S. Williams[a,b,c,d,2]

[a]Department of Ophthalmology and Stein Eye Institute, University of California, Los Angeles (UCLA), Los Angeles, CA 90095; [b]Department of Neurobiology, David Geffen School of Medicine, UCLA, Los Angeles, CA 90095; [c]Molecular Biology Institute, UCLA, Los Angeles, CA 90095; and [d]Brain Research Institute, UCLA, Los Angeles, CA 90095

Edited by Robert E. Anderson, University of Oklahoma Health Sciences Center, Oklahoma City, OK, and accepted by Editorial Board Member Jeremy Nathans April 12, 2018 (received for review June 8, 2017)

Stargardt macular dystrophy 3 (STGD3) is caused by dominant mutations in the *ELOVL4* gene. Like other macular degenerations, pathogenesis within the retinal pigment epithelium (RPE) appears to contribute to the loss of photoreceptors from the central retina. However, the RPE does not express *ELOVL4*, suggesting photoreceptor cell loss in STGD3 occurs through two cell nonautonomous events: mutant photoreceptors first affect RPE cell pathogenesis, and then, second, RPE dysfunction leads to photoreceptor cell death. Here, we have investigated how the RPE pathology occurs, using a STGD3 mouse model in which mutant human ELOVL4 is expressed in the photoreceptors. We found that the mutant protein was aberrantly localized to the photoreceptor outer segment (POS), and that resulting POS phagosomes were degraded more slowly in the RPE. In cell culture, the mutant POSs are ingested by primary RPE cells normally, but the phagosomes are processed inefficiently, even by wild-type RPE. The mutant phagosomes excessively sequester RAB7A and dynein, and have impaired motility. We propose that the abnormal presence of ELOVL4 protein in POSs results in phagosomes that are defective in recruiting appropriate motor protein linkers, thus contributing to slower degradation because their altered motility results in slower basal migration and fewer productive encounters with endolysosomes. In the transgenic mouse retinas, the RPE accumulated abnormal-looking phagosomes and oxidative stress adducts; these pathological changes were followed by pathology in the neural retina. Our results indicate inefficient phagosome degradation as a key component of the first cell nonautonomous event underlying retinal degeneration due to mutant ELOVL4.

photoreceptor | ELOVL4 | Stargardt | phagocytosis

Autosomal dominant Stargardt macular dystrophy 3 (STGD3) results in early loss of central vision from photoreceptor degeneration. It is caused by single allelic mutations in the *elongation of very long-chain fatty acids 4* (*ELOVL4*) gene (1, 2). This gene encodes a transmembrane enzyme that catalyzes the condensation reaction in the elongation of very long chain saturated (VLC-FA) and polyunsaturated fatty acids (VLC-PUFA) greater than 26 carbons (3). STGD3-associated mutations generate truncated forms of the ELOVL4 protein that lack the endoplasmic reticulum (ER) retention signal present at the C terminus of the protein (1, 4, 5).

Studies have attempted to identify how this defect leads to the death of the photoreceptor cells in dominant Stargardt disease. Cell culture studies suggested that mutant ELOVL4 interacts with wild-type (WT) ELOVL4, such that the WT protein is mislocalized from the ER, and lacks enzymatic activity (6). However, in frog and mammalian photoreceptors that expressed mutant and WT *ELOVL4*, the WT ELOVL4 protein appeared to be localized normally (7–10). Moreover, the retinas of transgenic mice, expressing mutant human *ELOVL4*, the TG(mut*ELOVL4*)2 line, which closely resembles human STGD3 (11), contain WT levels of VLC-PUFA, indicating that the mutant ELOVL4 does not affect the function of the WT protein (12).

Mouse models that include the knockin of a mutant *Elovl4*, to generate *Elovl4*$^{+/mut}$, as well as the TG(mut*ELOVL4*)2 mice, show RPE pathology preceding photoreceptor cell death (10, 11, 13, 14). As in other forms of macular degeneration, including STGD1 (15) and age-related macular degeneration (AMD) (16), RPE pathology in STGD3 appears to be a significant, if not the main contributor to photoreceptor cell degeneration (10, 11).

Cell nonautonomous toxicity has widespread importance for neurodegenerations, although the underlying cellular mechanisms are largely unknown. They have been reported to contribute to diseases, such as Alzheimer's, Parkinson's, and Huntington's disease, as well as amyotrophic lateral sclerosis, in which neuronal damage is promoted by mutant gene expression in neighboring cell types (reviewed in ref. 17). In the case of retinal degeneration in STGD3, the cell nonautonomous pathway appears to be unusually complex, with the involvement of an additional step. The RPE does not express *ELOVL4* (3, 12), suggesting that its contribution to photoreceptor degeneration

Significance

Cell nonautonomous toxicity is involved in various neurodegenerations, but mechanistic understanding is limited. Here, we provide insight into cellular mechanisms underlying a dominant macular degeneration, which results from mutant *ELOVL4*, and represents an unusual case of two separate cell nonautonomous events. We demonstrate that the first event involves RPE phagocytosis of photoreceptor disc membranes that contain mislocalized mutant ELOVL4 protein. We show that the mutant phagosomes are degraded inefficiently, thus introducing toxicity to the RPE. This leads to the second event involving perturbed retinal homeostasis of the neural retina and photoreceptor degeneration. In addition, our results provide a unique demonstration that phagosome content affects phagosome motility and that the motility of the phagosome, specifically, may be critical for its timely degradation.

Author contributions: J.E.-R., R.A.H., T.D., and D.S.W. designed research; J.E.-R., R.A.H., T.D., A.E.P., S.V., and A.U. performed research; J.E.-R., R.A.H., T.D., A.E.P., S.V., A.U., and D.S.W. analyzed data; and J.E.-R., R.A.H., and D.S.W. wrote the paper.

The authors declare no conflict of interest.

This article is a PNAS Direct Submission. R.E.A. is a guest editor invited by the Editorial Board.

[1]J.E.-R. and R.A.H. contributed equally to this work.

[2]To whom correspondence should be addressed. Email: dswilliams@ucla.edu.

This article contains supporting information online at www.pnas.org/lookup/suppl/doi:10.1073/pnas.1709211115/-/DCSupplemental.

Published online May 7, 2018.

in STGD3 stems from RPE pathogenesis that was originally introduced from the photoreceptors themselves.

Here, we explored the first cell nonautonomous step in STGD3: how mutant ELOVL4 in the photoreceptors may lead to RPE pathology. We focused on a major function of the RPE, involving the phagocytosis of the distal POS discs (18, 19), which, in mammals, amounts to 10% of the POS discs each day (20). Each RPE cell serves many photoreceptors (more than 200 in mouse) (21), so that disc membrane degradation represents a heavy metabolic load. We demonstrate that POSs of *ELOVL4*-mutant photoreceptors contain mislocalized mutant ELOVL4 protein, and that phagosomes of these POSs are degraded more slowly by the RPE. We present evidence that the presence of ELOVL4 protein in phagosomes affects their association with RAB7A and their recruitment of cytoplasmic dynein, resulting in impaired motility, which underlies their retarded degradation. Our findings have major implications for understanding phagocytosis by demonstrating the importance of the content of ingested material on phagosome motility, and by indicating that impaired phagosome motility, in an otherwise normal cell, appears sufficient to retard degradation.

Results

Photoreceptor Degeneration and Localization of WT and Mutant ELOVL4. Our line of transgenic mice, expressing mutant human *ELOVL4*, originates from the TG(mut*ELOVL4*)2 line (referred to as simply TG2 hereafter), as described previously (11). At 21 d old (P21), no photoreceptor loss was evident, but by P70 it is quite significant (Fig. 1 *A*–*D*). Quantification of the number of photoreceptor nuclei in the outer nuclear layer showed that at P45 and at P70, ∼20% and ∼50%, respectively, of the photoreceptors had been lost in the TG2 retinas (Fig. 1*E*).

By qPCR, we determined the expression of the mutant transgene to be three times that of WT *Elovl4* in the TG2 line. Using an antibody that was raised against an ELOVL4 N-terminal antigen, and appears to label both WT and mutant ELOVL4 (*SI Appendix*, Fig. S1), we found that the POSs were labeled in TG2 but not in WT retinal sections (Fig. 1*F*), indicating that the mutant ELOVL4 protein is dislocalized to the outer segment.

To investigate mutant ELOVL4 localization further, we generated a plasmid construct containing a FLAG-tagged cDNA of human *ELOVL4* with the same 5-bp deletion as in the TG2 transgene (and as observed in STGD3 patients). The construct was electroporated into the photoreceptors of WT mice. FLAG antibody labeling showed the presence of the mutant ELOVL4 in the POSs. By contrast, electroporation of a construct containing FLAG-tagged WT ELOVL4 resulted in inner segment but not outer segment labeling (Fig. 1*H*). These results are consonant with findings from transgenic frog retinas (9).

Labeling of retinal sections with an ELOVL4 antibody raised against a C-terminal epitope, which does not recognize the truncated mutant protein, also indicated that the WT protein was absent from the POSs of TG2 retinas. Labeling of the WT protein was comparable between TG2 and WT retinas, in agreement with a previous report (12). It was present mainly in the inner segment, but

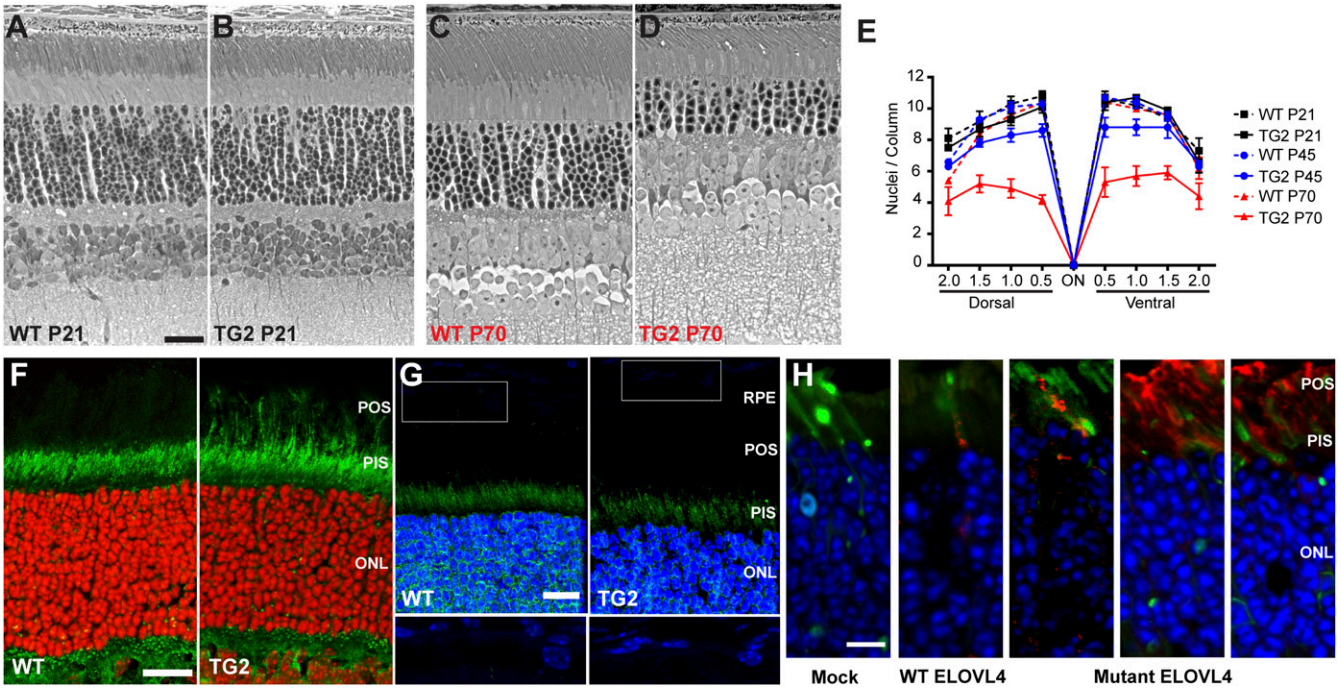

Fig. 1. Retinal degeneration and localization of ELOVL4. (*A*–*D*) Phase-contrast images of semithin sections from P21 or P70 WT (*A* and *C*) and TG2 (*B* and *D*) retinas. Mutant TG2 retinas were similar in overall morphology to WT retinas at P21, but the photoreceptor cells have undergone markedly significant degeneration by P70, as can be observed by the loss of photoreceptor nuclei in the outer nuclear layer (ONL). (*E*) Graph of the number of photoreceptor nuclei per column in the ONL, quantified at 0.5-mm intervals from the optic nerve (ON). Some photoreceptor cell loss in TG2 retinas was observed at P45; by P70 it was more severe. (*F* and *G*) Retinal sections from P21 WT and TG2 mice immunolabeled with antibodies against the N-terminal (*F*) or C-terminal (*G*) region of ELOVL4 (green). The N-terminal antibody recognizes both WT and mutant ELOVL4, but the C-terminal antibody recognizes only WT ELOVL4. Photoreceptor outer segments (POSs) are labeled in the TG2 retinal section by the former (*F*), but not the latter (*G*). Nuclei were counterstained with DAPI (shown as red or blue). *Lower* panels (*G*) represent higher magnification of rectangles in *Upper* panels, with the brightness of the blue channel increased to make weaker DAPI staining of RPE cells visible. (*H*) Retinal sections from mice whose photoreceptors were electroporated with Dendra2 (green) and FLAG-tagged WT or mutant human *ELOVL4* plasmids. The sections were labeled with a FLAG antibody (red). Mock retinas were electroporated with Dendra2 only. The WT FLAG-ELOVL4 protein is localized primarily to the photoreceptor inner segment (PIS). The three panels to the *Right* are examples from different experiments with the mutant FLAG-*ELOVL4*; protein was observed mostly in the POS, with some presence in the PIS (mutant ELOVL4 still contains the N-terminal ER localization signal, but it has lost the C-terminal ER retention signal). (Scale bars: 10 μm in *A*, *F*, and *H*, and 15 μm in *G*.)

also with suggestion of label in the outer nuclear and outer plexiform layers (Fig. 1*G*), as reported previously (3, 7, 10). These results indicate that the localization of the TG2 protein to the POS does not significantly affect the localization of the WT protein.

WT ELOVL4 is not detectable in the RPE (Fig. 1*G*). However, a consequence of mutant ELOVL4 dislocalization to the POSs is that phagosomes within the TG2 RPE should contain mutant ELOVL4. These phagosomes could be detected with the N-terminal ELOVL4 antibody (*SI Appendix*, Fig. S2).

Delayed Degradation of Phagosomes from TG2 Outer Segments. By electron microscopy, we observed previously that the RPE of TG2 retinas accumulate membranous debris and lipid droplets over time (11), suggestive of a defect in POS degradation. To test whether such a defect underlies the pathology of TG2 retinas, we analyzed the rate of degradation in young mouse retinas, showing no pathology or degeneration. First, we imaged phagosomes in the RPE of P21 mice at 0.5 h post light onset, the peak of phagocytosis in mice, and at 3 h after light onset, when the number of phagosomes in the RPE of WT retinas has been significantly reduced due to degradation (22, 23) (Fig. 2 *A*–*D*). The number of POS phagosomes in TG2 retinas was comparable to that in WT retinas at 0.5 h, indicating that the rate and timing of ingestion appear to be normal. However, at 3 h after light onset, the number is significantly greater in TG2 retinas, indicating only a minor decrease from 0.5 h after light onset (Fig. 2*E*) and suggesting either defective degradation or additional ingestion. Given that the POS length was unchanged between the two time points, our results support the former.

We also examined POS phagosome degradation, using an in vitro pulse-chase assay with primary cultures of RPE cells from WT mice, an approach that enabled us to examine acute effects in the RPE due to the presence of mutant ELOVL4 in the POSs. We purified POSs from the retinas of WT and TG2 littermates (Fig. 3*A*), fed them to the WT primary mouse RPE cells for 10 min, and washed the cells extensively to remove unbound POSs. The cells were then fixed either immediately (pulse), or after an additional 2-h period (chase). Rod opsin (RHO) double immunolabeling (before and after cell permeabilization) was then performed to differentiate between POSs bound to the surface of the RPE and POSs ingested by the RPE (Fig. 3*B*). The number of surface-bound POSs was not significantly different between WT and TG2 after the pulse and chase period (Fig. 3*C*). Furthermore, the number of ingested POSs was also not significantly different after the pulse (Fig. 3*D*, *Left*). Thus, the binding and ingestion of TG2 POSs appeared to be normal. However, a significant difference in the number of POSs was observed after the 2-h chase period, at which point, the RPE cells fed WT POSs had degraded ~40% of their ingested POS phagosomes, whereas the RPE cells fed TG2 POSs showed no significant decrease in their POS phagosome content (Fig. 3*D*, *Right*). This result indicates that WT primary mouse RPE cells do not degrade phagosomes originating from TG2 POSs as efficiently as phagosomes from WT POSs.

Newly formed POS phagosomes are labeled by antibodies against both the N and C termini of RHO. However, labeling by RHO mAb1D4, which recognizes a C-terminal epitope, is lost quickly as phagosomes begin to mature, so that it is a specific marker for immature phagosomes (24, 25). Using mAb1D4, our results showed that the number of immature WT and TG2 phagosomes was similar (Fig. 3*E*). The slower degradation rate was evident only with TG2 phagosomes that were more mature (Fig. 3*F*), indicating that initial phagosome maturation proceeds normally.

We also tested whether this phenotype could be replicated in human RPE cells using the ARPE-19 immortalized cell line. ARPE-19 cells were challenged with either WT or TG2 POSs for 4 h, washed extensively, and fixed immediately or after a 3-h or

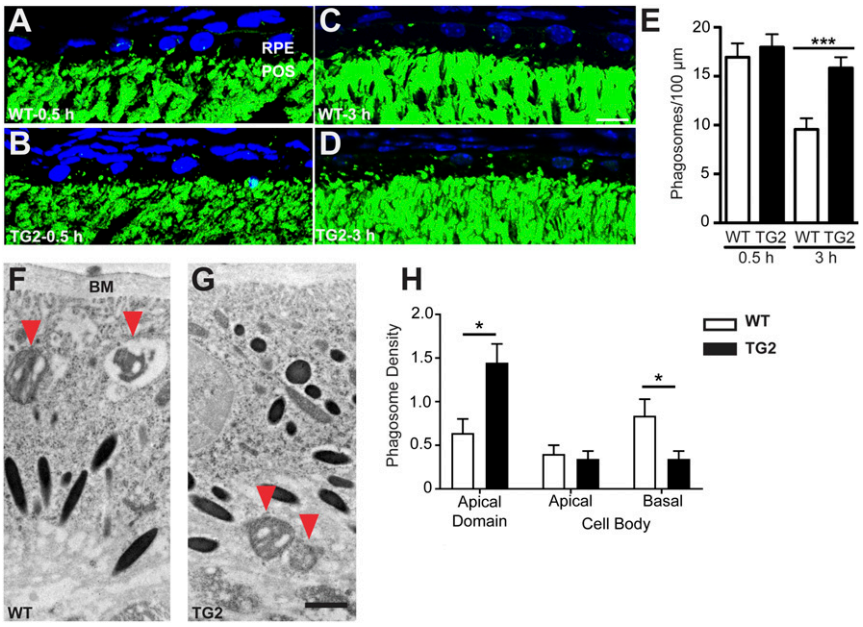

Fig. 2. Degradation of POS phagosomes in WT and mutant mouse RPE in vivo. (*A*–*D*) Immunofluorescence images of RHO labeling (green) in WT (*A* and *C*) and TG2 (*B* and *D*) retinal sections from P21 mice killed 0.5 h (*A* and *B*) and 3 h (*C* and *D*) post light onset. POS phagosomes can be seen as green particles in the RPE layer. The nuclei are counterstained with DAPI (blue). (*E*) Quantification of POS phagosomes per 100 μm of the RPE layer in WT and TG2 retinas showed no significant difference at 0.5 h post light onset, but significantly more POS phagosomes remained in TG2 RPE at 3 h post light onset, indicating impaired phagosome degradation. (*F* and *G*) ImmunoEMs of WT (*F*) and TG2 (*G*) retinas from P28 mice showing POS phagosomes (immunogold labeled with RHO antibodies, and indicated by red arrowheads) inside the RPE at 1.5 h post light onset. (*H*) Quantification of phagosome density (mean number of phagosomes per 55 μm^2 of sectioned RPE) in different regions of the RPE. Bar graph shows data from the apical and cell body domains of the RPE; these domains border each other at the level of the junctional complexes. The cell body domain was divided further into apical and basal halves. The data show that more TG2 than WT POS phagosomes were in the apical domain, while more WT than TG2 phagosomes were in the basal half of the cell body. BM, Bruch's membrane. (Scale bars in *C* and *G*: 10 μm and 1 μm, respectively.) Error bars in *E* and *H* represent ±SEM. $*P < 0.05$; $***P < 0.001$.

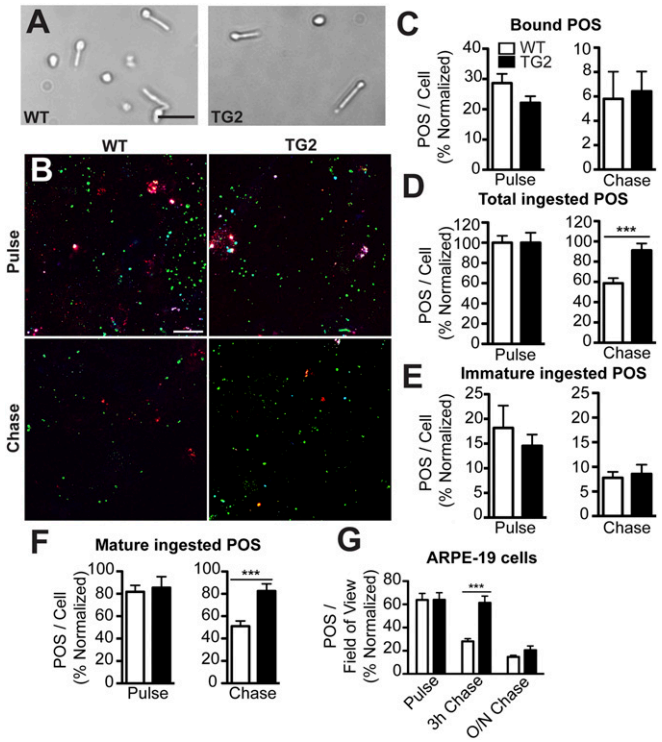

Fig. 3. Impaired degradation of mutant ELOVL4 POSs by WT RPE cultures. (*A*) Brightfield images of WT and TG2 POSs isolated from respective retinas. (*B*) RHO labeling of WT primary mouse RPE cells, fed either WT or TG2 POSs, immediately following the pulse or following a chase period. The labeling was performed before and after cell permeabilization to distinguish between surface-bound POSs (white or red) and internalized phagosomes. Additionally, the immature phagosomes (cyan) were identified by labeling with a RHO mAb that binds the C terminus (1D4) and RHO pAb01, while the mature phagosomes (green) were identified by labeling with RHO pAb01 only. (*C–F*) Quantification of the POSs. POSs fed to primary mouse RPE and labeled with RHO pAb01, showed that there was no significant difference between the number of bound POSs after the pulse and chase (*C*), but there were more total ingested TG2 POSs following the chase compared with WT POSs (*D*). When the total POSs were further defined as immature (labeled with mAb1D4) vs. mature (labeled with pAb01 but not mAb1D4), the number of immature ingested POSs was not found to be statistically significant between WT and TG2 POSs (*E*), whereas the cells fed TG2 POSs had more mature ingested POSs following the chase (*F*). (*G*) The impaired POS degradation phenotype was also observed in human ARPE-19 cells, which after a 3-h chase period, had more (bound + ingested) TG2 POSs than ARPE-19 cells fed WT POSs. O/N, overnight. (Scale bars in *A* and *B*: 20 μm and 10 μm, respectively.) Error bars in *C–G* represent ±SEM. ***$P < 0.001$.

16-h chase period. ARPE-19 cells showed a decrease in phagosomes between the pulse and 3-h chase period when fed WT POSs. In contrast, the phagosome content was not significantly different between the pulse and 3-h chase period when the cells were fed TG2 POSs (Fig. 3*G*). This result confirms that the delay in degradation of TG2 phagosomes, observed in mouse primary RPE cells, can be phenocopied in these human RPE cells. Interestingly, the numbers of phagosomes in ARPE-19 cells fed WT and TG2 POSs were similar after the 16-h chase period, indicating that the degradation of phagosomes from TG2 POSs is not completely inhibited, but occurs at a slower rate than that of phagosomes from WT POSs.

TG2 POS Phagosome Trafficking. Phagosome maturation and degradation is associated with an apical-to-basal migration through the RPE (26). In previous studies, we have found that POS phagosome degradation is affected by molecular motor function in the RPE. Mutations in the actin-based motor, myosin-7a (22), and the microtubule-based motor, kinesin-1 (27), lead to impaired POS phagosome motility, slower basal migration, and less efficient degradation by the RPE. We therefore tested whether impaired phagosome motility and migration might be a contributor to the delayed degradation of TG2 POS phagosomes.

Using electron microscopy to gauge the distribution of phagosomes in the RPE of WT and TG2 retinas, we found that at 1.5 h after light onset, the majority of TG2 phagosomes were in the apical region of the RPE, while significantly more WT phagosomes were localized basally in the RPE, near Bruch's membrane (Fig. 2 *F–H*). These results suggest that TG2 phagosomes progress more slowly along the apical–basal axis of the RPE, thereby resulting in their delayed degradation.

Next, we used live-cell imaging of WT and TG2 phagosomes in WT primary RPE cultures. Analysis of phagosome motility tracks (Movie S1) revealed that TG2 phagosomes had a significantly slower average velocity than WT phagosomes. The majority (78%) of WT phagosomes exhibited average velocities between 0.4 and 0.8 μm/s, whereas only 39% of TG2 phagosomes exhibited average velocities in this range (Fig. 4*A*). We also analyzed the distance phagosomes traveled between pauses (i.e., instantaneous velocity ≤0.1 μm/s), and defined this parameter as run length (*SI Appendix*, Fig. S3). Previously, we had observed that this motility parameter was compromised, together with phagosome degradation rate, in RPE lacking a kinesin-1 light chain (27). Analysis revealed that TG2 phagosomes have a significantly shorter mean run length relative to WT phagosomes (1.3 μm vs. 1.9 μm, respectively) (Fig. 4*B*). Taken together, these results suggest that TG2 phagosomes have impaired motility in live RPE cells, as indicated by the lower mean velocity and by movements that are less productive, as indicated by the shorter run lengths. Note that this defect can be attributed specifically to the POS phagosomes, since the RPE cells were WT, in which the motor protein function, as well as the motility of organelles, such as endolysosomes, should be normal.

RAB7A and Dynein Motor Association with TG2 POS Phagosomes. We focused on the phagosomes themselves to identify characteristics that might underlie their defective motility. We tested whether the ELOVL4-containing mutant phagosomes showed abnormal association with motor protein linkers. Although we detected no significant difference between WT and TG2 phagosomes in their association with RAB5, there was a marked difference in RAB7A association. WT primary mouse RPE cells were challenged with WT or TG2 POSs for 20 min and, following a 1-h chase period, were fixed and labeled with antibodies against RHO (mAb4D2) and RAB7A (Fig. 4*C*). A colocalization analysis was performed to evaluate the association of WT and TG2 phagosomes (mAb4D2 labeled) with RAB7A. We found that ∼27% of the TG2 phagosomes, but only 10% of WT phagosomes were also labeled with RAB7A antibodies (Fig. 4*D*). These results suggest that phagosomes, derived from TG2 POSs, more readily sequester RAB7A, which may alter their association with motor proteins, and subsequently interfere with their motility, thereby contributing to the slower rate of degradation.

To test for altered motor protein recruitment to these mutant phagosomes, we evaluated their association with dynein. After feeding WT or TG2 POSs to WT RPE cells, we quantified the proportion of POS phagosomes, labeled with anti-RHO, that were also labeled with antibodies against cytoplasmic dynein intermediate chain (DIC) (Fig. 4*E*). The mean proportion of TG2 POS phagosomes that were associated with DIC was higher than that of WT POS phagosomes (Fig. 4*F*). These results implicate increased sequestration of RAB7A in abnormal linkage of TG2 phagosomes to the dynein motor protein, which may affect the balance between dynein and kinesin motors, thus contributing to impaired motility of these organelles.

CELL BIOLOGY

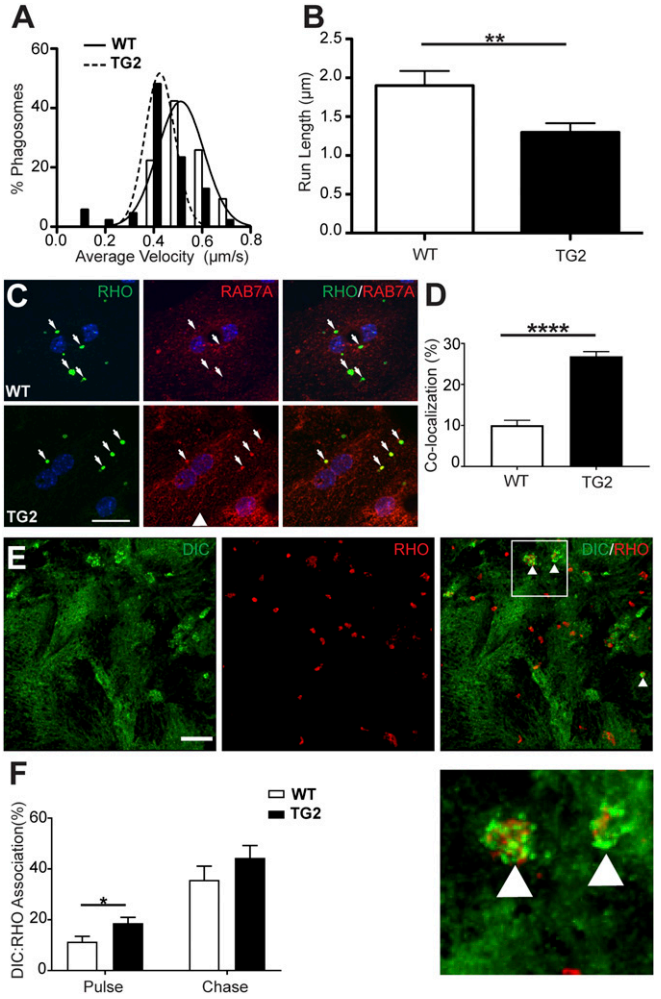

Fig. 4. Impaired motility of TG2 phagosomes in WT primary mouse RPE cells. (*A* and *B*) Live-cell analysis of the tracks of phagosomes (85 per condition), from either WT or TG2 POSs, showed that TG2 phagosomes had a lower mean velocity (*A*) and shorter mean run length (*B*) than their WT counterparts. (*C*) Immunolabeling of RHO (green) and the endosomal marker RAB7A (red) in WT primary mouse RPE cells, fed either WT or TG2 POSs. (*D*) Quantification of the number of RHO-positive phagosomes colocalized with RAB7A showed that more phagosomes, derived from TG2 POSs relative to WT POSs, had RAB7A associated with them after a 1-h chase period. (*E*) Immunofluorescence of cytoplasmic dynein intermediate chain (DIC, green) and RHO (red) in WT primary mouse RPE cells fed POSs after a 1-h chase. White arrowheads in the merged panel indicate phagosomes associated with DIC immunolabeling, shown at higher magnification *Below*. (*F*) Quantification of the proportion of WT or TG2 POS phagosomes in WT primary mouse RPE cells that were associated with DIC immunolabel, after a 20-min pulse and a 1-h chase. (Scale bars in *C* and *E*: 20 μm and 5 μm, respectively.) Error bars in *B*, *D*, and *F* represent ±SEM. $*P < 0.05$; $**P < 0.01$; $****P < 0.0001$.

Pathogenesis and Degeneration. In older TG2 and *Elovl4*$^{+/mut}$ knockin mice, membranous debris and vacuoles are evident in the RPE (10, 11, 13, 14), consistent with inefficient POS phagosome clearance over time. Here, we examined the RPE in young TG2 mice, to see if we could identify any early pathological changes. By electron microscopy, we observed clusters of membrane that looked like abnormal phagosomes, in the RPE of P21 TG2 mice (*SI Appendix*, Fig. S4). At this age, we also noted changes that we suspect are secondary changes and are indicative of a general decline in RPE health. First, some of the tight junction protein, zona occludens 1 (ZO-1), had lost its junctional localization, with an increase in immunoreactivity evident throughout the cytosol of TG2 RPE cells (*SI Appendix*, Fig. S5). This change is likely to lead to a decrease in epithelial barrier function, due to a breakdown in the intercellular junctions between RPE cells. Second, in older animals (P70), we observed a marked increase in oxidative stress in the RPE in vivo (*SI Appendix*, Fig. S6). Labeling for the oxidative stress marker, 4-HNE, was also increased in WT primary mouse RPE cells that were incubated with TG2 POSs (*SI Appendix*, Fig. S7).

These abnormalities in the RPE appear to be symptoms of RPE pathogenesis, resulting from cell stress evoked by inefficient degradation of POS phagosomes and likely contribute to the initiation of the second cell nonautonomous step, which negatively affects the health of the neural retina, leading to photoreceptor degeneration in TG2 mice. At the time that photoreceptor cell loss is first detected, around P45 (Fig. 1*E*), perturbed retinal homeostasis is evident by the invasion of microglia into the subretinal space (*SI Appendix*, Fig. S8).

Discussion

Mechanisms underlying retinal degeneration due to dominant mutations in *ELOVL4* have remained a puzzle, despite numerous cell culture and mouse model studies. As for most other forms of macular degeneration, RPE pathogenesis has been implicated (10, 11). However, the RPE does not express ELOVL4 (3, 12) (Fig. 1*G*). In the present study, we describe cellular mechanisms that account for RPE pathogenesis. Our results indicate that mutant ELOVL4 protein localizes abnormally to the outer segments of photoreceptor cells and passes to the RPE cells in phagosomes, as a result of the normal daily process of phagocytosis. We found that the ELOVL4-containing phagosomes are degraded less efficiently by the RPE cells, thus introducing toxicity to these professional phagocytes. We propose that observed defects in phagosome motility contribute to the retarded phagosome degradation, and that the impaired motility is possibly due to abnormal sequestration of RAB7A, which alters the association of the phagosome with the dynein motor protein (28, 29).

Cell nonautonomous effects are common in neurodegenerations (17). However, the pathogenesis associated with STGD3 maculopathy is highly unusual, due to two cell nonautonomous effects. The toxicity introduced to the RPE by phagocytosis of ELOVL4-containing POS disc membranes represents the first of the two. The subsequent effects on the neural retina, including photoreceptor cell loss, due to RPE pathology represents the second. There are some similarities with STGD1 maculopathy, which is also characterized by RPE defects, and ensuing photoreceptor cell loss. STGD1 is caused by recessive mutations in *ABCA4* (30). However, unlike *ELOVL4*, *ABCA4* is expressed by the RPE as well as the photoreceptor cells, and the in vivo RPE pathogenesis of STGD1 appears to be largely cell autonomous (31).

How does the presence of ELOVL4 protein alter the disc membranes so that POS phagosomes interact differently with RAB7A and are degraded more slowly by WT RPE? The C-terminal truncated mutant ELOVL4, as expressed in TG2, has lost its ER retention motif, but it still contains a normal catalytic region, suggesting that its presence in the TG2 disc membranes might result in additional very long chain fatty acids. On the other hand, no difference in levels of retinal VLC-PUFAs was detected between WT and TG2 retinas (12), and tests of the mutant ELOVL4 enzyme detected no activity (6), suggesting that the POS membranes may be affected solely by the abnormal presence of the mutant (transmembrane) protein. Indeed, the presence of mutant ELOVL4 protein in the POSs appears capable of altering disc membrane organization of the POSs, if at a high enough concentration. In a transgenic mouse line that expresses mutant *ELOVL4* at 60% higher levels than that in the TG2 line, the discs are not stacked normally and appear disorganized, in contrast to the disc membranes in the TG2 mice, which appear normal by electron microscopy (11).

In the TG2 mice, a defect in the POS membranes became evident once the membranes had been ingested by the RPE. The altered behavior of the TG2 POS phagosomes, as described here, emphasizes that the content of a phagosome can have a significant effect on the ability of a phagosome to associate with proteins that influence its maturation, including motor-linking proteins and thus the motor proteins themselves. Initially, the outer membrane of a phagosome comes from the plasma membrane of the phagocyte. However, phagosomes, including POS phagosomes (25), undergo a series of fusion–fission events with endolysosomes as they mature, resulting in drastic remodeling of the phagosomal membrane and contents (32). Particularly, when the ingested material contains a high concentration of membranes, as in the case of a POS phagosome, the observed membrane coalescence (33) is likely to involve a mixing of membranes that results in an outer membrane that contains components of the ingested membrane. The content of a membrane affects motor protein association (29, 34, 35). For example, increased cholesterol in the membrane of motor protein cargoes has been shown to increase RAB7 association, which results in more dynein and less kinesin activity (28). RAB7 interacts with the cholesterol sensor, ORP1L (36) and was found recently to associate with cholesterol and dynein in microdomains on the surface of latex bead phagosomes (29). Understanding the molecular perturbation in the membrane of POS phagosomes from TG2 mice is likely to further our understanding of molecular motor linkage and regulation.

The importance of phagosome motility for degradation was suggested from studies illustrating mislocalized and immature POS phagosomes in the opossum RPE after intraocular treatment with colchicine, which inhibits microtubule polymerization (37). Subsequently, impairment of POS phagosome motility and degradation was found in the RPE of mice lacking the actin motor protein, myosin-7a (22), or the light chain of the microtubule motor protein, kinesin-1 (27). However, phagosome degradation is likely dependent upon the motility of other organelles, especially endolysosomes (38), so that the specific impact of impaired phagosome motility on phagosome degradation cannot be determined by altering motility throughout the RPE cell. In the present cell culture studies, where mutant TG2 POSs were fed to WT RPE cells, we were able to pinpoint the motility defect specifically to the phagosome organelle, and thus demonstrate the importance of the motility of the phagosome per se.

Materials and Methods

Animal use followed NIH guidelines, and was in accordance with the University of California, Los Angeles Institutional Animal Care and Use Committee under an approved protocol. A detailed description of mice, cell culture, phagocytosis assays, immunofluorescence, live-cell imaging, other microscopy, and statistical analyses is provided in *SI Appendix, SI Materials and Methods*.

ACKNOWLEDGMENTS. We thank Barry Burgess for technical assistance; Roxana Radu for discussions; Kang Zhang for kindly providing retinal tissues at the start of the project; and Martin-Paul Agbaga and Robert E. Anderson for kindly providing ELOVL4 antibodies, viral constructs, TG2 mouse breeders, as well as helpful comments. The study was supported by National Institutes of Health Grants F31EY026805 (to R.A.H.), R01EY013408 and R01EY027442 (to D.S.W.), and P30EY000331.

1. Zhang K, et al. (2001) A 5-bp deletion in ELOVL4 is associated with two related forms of autosomal dominant macular dystrophy. *Nat Genet* 27:89–93.
2. Edwards AO, Donoso LA, Ritter R, 3rd (2001) A novel gene for autosomal dominant Stargardt-like macular dystrophy with homology to the SUR4 protein family. *Invest Ophthalmol Vis Sci* 42:2652–2663.
3. Agbaga MP, et al. (2008) Role of Stargardt-3 macular dystrophy protein (ELOVL4) in the biosynthesis of very long chain fatty acids. *Proc Natl Acad Sci USA* 105:12843–12848.
4. Bernstein PS, et al. (2001) Diverse macular dystrophy phenotype caused by a novel complex mutation in the *ELOVL4* gene. *Invest Ophthalmol Vis Sci* 42:3331–3336.
5. Maugeri A, et al. (2004) A novel mutation in the ELOVL4 gene causes autosomal dominant Stargardt-like macular dystrophy. *Invest Ophthalmol Vis Sci* 45:4263–4267.
6. Logan S, et al. (2013) Deciphering mutant ELOVL4 activity in autosomal-dominant Stargardt macular dystrophy. *Proc Natl Acad Sci USA* 110:5446–5451.
7. Grayson C, Molday RS (2005) Dominant negative mechanism underlies autosomal dominant Stargardt-like macular dystrophy linked to mutations in ELOVL4. *J Biol Chem* 280:32521–32530.
8. Sommer JR, et al. (2011) Production of ELOVL4 transgenic pigs: A large animal model for stargardt-like macular degeneration. *Br J Ophthalmol* 95:1749–1754.
9. Agbaga MP, et al. (2014) Mutant ELOVL4 that causes autosomal dominant stargardt-3 macular dystrophy is misrouted to rod outer segment disks. *Invest Ophthalmol Vis Sci* 55:3669–3680.
10. Kuny S, Cho WJ, Dimopoulos IS, Sauvé Y (2015) Early onset ultrastructural and functional defects in RPE and photoreceptors of a Stargardt-like macular dystrophy (STGD3) transgenic mouse model. *Invest Ophthalmol Vis Sci* 56:7109–7121.
11. Karan G, et al. (2005) Lipofuscin accumulation, abnormal electrophysiology, and photoreceptor degeneration in mutant ELOVL4 transgenic mice: A model for macular degeneration. *Proc Natl Acad Sci USA* 102:4164–4169.
12. Mandal NA, et al. (2014) In vivo effect of mutant ELOVL4 on the expression and function of wild-type ELOVL4. *Invest Ophthalmol Vis Sci* 55:2705–2713.
13. Vasireddy V, et al. (2006) Elovl4 5-bp-deletion knock-in mice develop progressive photoreceptor degeneration. *Invest Ophthalmol Vis Sci* 47:4558–4568.
14. Vasireddy V, et al. (2009) Elovl4 5-bp deletion knock-in mouse model for Stargardt-like macular degeneration demonstrates accumulation of ELOVL4 and lipofuscin. *Exp Eye Res* 89:905–912.
15. Weng J, et al. (1999) Insights into the function of Rim protein in photoreceptors and etiology of Stargardt's disease from the phenotype in abcr knockout mice. *Cell* 98:13–23.
16. Ambati J, Atkinson JP, Gelfand BD (2013) Immunology of age-related macular degeneration. *Nat Rev Immunol* 13:438–451.
17. Ilieva H, Polymenidou M, Cleveland DW (2009) Non-cell autonomous toxicity in neurodegenerative disorders: ALS and beyond. *J Cell Biol* 187:761–772.
18. Young RW, Bok D (1969) Participation of the retinal pigment epithelium in the rod outer segment renewal process. *J Cell Biol* 42:392–403.
19. Williams DS, Fisher SK (1987) Prevention of the shedding of rod outer segment disks by detachment from the retinal pigment epithelium. *Invest Ophthalmol Vis Sci* 28:184–187.
20. Young RW (1967) The renewal of photoreceptor cell outer segments. *J Cell Biol* 33:61–72.
21. Volland S, Esteve-Rudd J, Hoo J, Yee C, Williams DS (2015) A comparison of some organizational characteristics of the mouse central retina and the human macula. *PLoS One* 10:e0125631.
22. Gibbs D, Kitamoto J, Williams DS (2003) Abnormal phagocytosis by retinal pigmented epithelium that lacks myosin VIIa, the Usher syndrome 1B protein. *Proc Natl Acad Sci USA* 100:6481–6486.
23. Sethna S, et al. (2016) Regulation of phagolysosomal digestion by caveolin-1 of the retinal pigment epithelium is essential for vision. *J Biol Chem* 291:6494–6506.
24. Esteve-Rudd J, Lopes VS, Jiang M, Williams DS (2014) In vivo and in vitro monitoring of phagosome maturation in retinal pigment epithelium cells. *Adv Exp Med Biol* 801:85–90.
25. Wavre-Shapton ST, Meschede IP, Seabra MC, Futter CE (2014) Phagosome maturation during endosome interaction revealed by partial rhodopsin processing in retinal pigment epithelium. *J Cell Sci* 127:3852–3861.
26. Herman KG, Steinberg RH (1982) Phagosome movement and the diurnal pattern of phagocytosis in the tapetal retinal pigment epithelium of the opossum. *Invest Ophthalmol Vis Sci* 23:277–290.
27. Jiang M, et al. (2015) Microtubule motors transport phagosomes in the RPE, and lack of KLC1 leads to AMD-like pathogenesis. *J Cell Biol* 210:595–611.
28. Lebrand C, et al. (2002) Late endosome motility depends on lipids via the small GTPase Rab7. *EMBO J* 21:1289–1300.
29. Rai A, et al. (2016) Dynein clusters into lipid microdomains on phagosomes to drive rapid transport toward lysosomes. *Cell* 164:722–734.
30. Allikmets R, et al. (1997) A photoreceptor cell-specific ATP-binding transporter gene (ABCR) is mutated in recessive Stargardt macular dystrophy. *Nat Genet* 15:236–246.
31. Lenis TL, et al. (2017) Expression of ABCA4 in retinal pigment epithelium cells and its implications for Stargardt disease. *Invest Ophthalmol Vis Sci ARVO E-Abstr* 607.
32. Vieira OV, Botelho RJ, Grinstein S (2002) Phagosome maturation: Aging gracefully. *Biochem J* 366:689–704.
33. Young RW (1971) The renewal of rod and cone outer segments in the rhesus monkey. *J Cell Biol* 49:303–318.
34. Klopfenstein DR, Tomishige M, Stuurman N, Vale RD (2002) Role of phosphatidylinositol(4,5)bisphosphate organization in membrane transport by the Unc104 kinesin motor. *Cell* 109:347–358.
35. Nelson SR, Trybus KM, Warshaw DM (2014) Motor coupling through lipid membranes enhances transport velocities for ensembles of myosin Va. *Proc Natl Acad Sci USA* 111:E3986–E3995.
36. Rocha N, et al. (2009) Cholesterol sensor ORP1L contacts the ER protein VAP to control Rab7-RILP-p150 Glued and late endosome positioning. *J Cell Biol* 185:1209–1225.
37. Herman KG, Steinberg RH (1982) Phagosome degradation in the tapetal retinal pigment epithelium of the opossum. *Invest Ophthalmol Vis Sci* 23:291–304.
38. Desjardins M, Huber LA, Parton RG, Griffiths G (1994) Biogenesis of phagolysosomes proceeds through a sequential series of interactions with the endocytic apparatus. *J Cell Biol* 124:677–688.